Experimental Study on the Heat Loss Mechanism in a Metal Containment Vessel under Various Gap Conditions during Normal Operation of a Small Modular Reactor

Geunyoung Byeon [a], JinHo Song [a], Sung Joong Kim [a,b*]
[a]*Department of Nuclear Engineering Hanyang University., 222 Wangsimni-ro, Seongdong-gu Seoul, Korea*
[b]*Institute of Nano Science and Technology, Hanyang University., 222 Wangsimni-ro, Seongdong-gu, Seoul, Korea*
[*]*Corresponding author: sungjkim@hanyang.ac.kr*

Keywords : Heat loss, Small modular reactor (SMR), Metal containment vessel (MCV), Radiative heat transfer, Natural convection

1. Introduction

Small modular reactors (SMRs) have gained global attention due to their enhanced safety features, modularity, and a wide range of applications in industries such as deep-water desalination, process heat production, and power generation [1-2]. SMRs under global development exhibit innovative designs such as integrated nuclear steam supply systems (NSSS). Among them, the noteworthy structure of some SMRs includes the metal containment vessel (MCV) structure, which surrounds the reactor pressure vessel (RPV).

The gap between the RPV and the MCV is a key element in the design of SMRs. It serves a crucial function during reactor normal operation, significantly reducing heat loss to the outside and effectively preventing MCV pressurization due to steam released from the RPV during reactor transients, such as automatic depressurization valve (ADV) operation.

Various SMRs under development fill the gap with different materials, including vacuum conditions or gases such as nitrogen and argon, to enhance the gap's effect. For example, NuScale VOYGR, developed by NuScale Power in the United States, and the i-SMR, developed by Korea Hydro & Nuclear Power in South Korea, have a vacuum condition (~0.07 bar) in the gap.

Adopting a vacuum condition to minimize convective heat transfer during normal operation could reduce heat losses compared to gas filling [3]. However, maintaining a vacuum condition has been a structural challenge for decades. As an alternative, GE-Hitachi's BWRX-300 uses sub-atmospheric nitrogen as the injected gas within the containment vessel [4]. Similarly, ARC CLEAN TECHNOLOGY's ARC-100 injects argon gas slightly above atmospheric pressure within the containment vessel [5]. Using inert gas in the containment atmosphere can dilute hydrogen and oxygen gases, which could be released during a severe accident, reducing the likelihood of an explosion [4-5].

In this study, we provide information on the temperature within the gap and the wall temperature during the normal operation of the i-SMR design. In reactor accident scenarios such as ADV stuck open, or loss of coolant accident (LOCA), the performance of condensation heat transfer is crucial to prevent overpressure in MCV caused by the released steam [6]. The performance of condensation heat transfer is primarily influenced by the temperature of the MCV wall, which acts as the condensation surface, as well as the temperature and steam and type of non-condensable gases inside [7]. However, since the initial conditions are expected to vary for each case, we provide information on the temperature in the gap between the RPV and MCV and the MCV wall temperature during reactor normal operation. Using the measured temperature data, we experimentally evaluated the critical heat transfer mechanisms to the external environment under different gap-filled conditions (argon, nitrogen, vacuum).

2. Methodology

This section describes the experimental equipment, measurement points, and test matrix.

2.1 Experimental apparatus

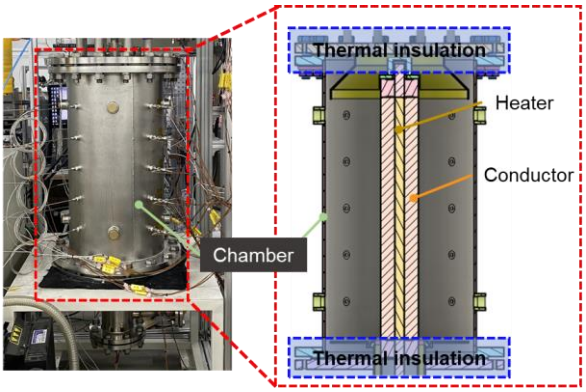

Fig. 1. Cross-section of a conjugate heat transfer experimental apparatus (before insulation)

Fig. 1 illustrates the experiment setup to evaluate total heat losses using heat transfer mechanisms in a reactor's steady state.

At the chamber's core, a cartridge heater with a diameter of 0.0254 m and a length of 0.85 m is surrounded by an aluminum conductor with an outer

diameter of 0.1016 m to replicate the RPV. The chamber measures 0.406m in outer diameter and 0.85m in height. The outer diameter was determined by considering the view factor at the height of the pressurizer in the i-SMR. In radiative heat transfer, the view factor and temperature are critical variables. According to previous studies, the temperature is highest at the pressurizer height in the i-SMR's RPV, so the geometry at this height was utilized.

In this study, the upper and lower flanges were insulated with ceramic fiber (Cerakwool), as shown in Fig. 1, to assess the amount of heat loss in the radial direction.

2.2 Measurement points

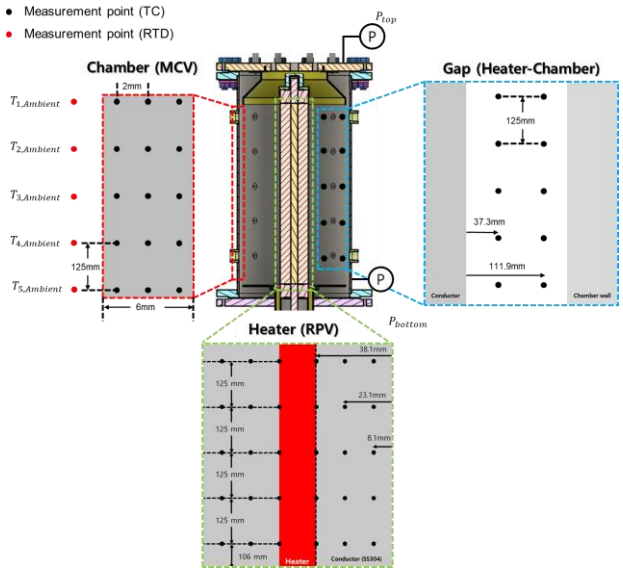

Fig. 2. Measurement points of the experimental apparatus (Heater, Gap, Chamber wall)

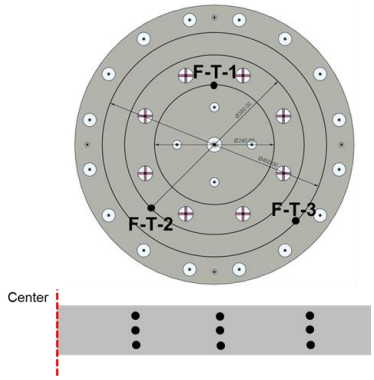

Fig. 3. Measurement points of the experimental apparatus (Upper flange)

Fig. 2 represents the pressure and temperature measurement points within the experimental setup.

There are two pressure transmitters, one at the top and one at the bottom of the chamber, to measure pressure.

The heater section is equipped with three K-type thermocouples at five different heights, placed at varying depths for temperature measurement. Additionally, in the space between the conductor and chamber wall, which simulates the SMR's gap, there are two K-type thermocouples at each of the five heights. The chamber wall, which simulates the SMR's MCV, has three K-type thermocouples at each of the five heights. Finally, five resistance temperature detectors (RTD) are placed outside the chamber wall to measure the ambient air temperature, one at each height.

As shown in Fig. 1, insulation was applied to the upper and lower flanges of the experimental chamber to prevent heat loss to the outside air. However, thermocouples were installed on the upper and lower flanges to calculate the overall heat balance, as depicted in Fig. 3. For the upper flange, three thermocouples were installed at three radial points, and for the lower flange, due to support structures, thermocouples were installed at two radial points, each at three different heights (same as F-T-1 and F-T-2 in Fig. 3).

2.3 Test matrix & Experimental procedure

The experiment was conducted under steady-state conditions to evaluate the heat loss from the MCV during normal reactor operation. Based on previous CFD research results, the surface temperature of the heater conductor was fixed at 320°C at the mid-height of the heater for all cases [8]. Unlike some currently developed SMR designs, this study assumed that the exterior of the MCV is cooled by air.

The experimental cases compared scenarios: one with Cerakwool insulation and the other with vacuum, nitrogen, and argon. Cerakwool was used to fill the gap to assess the amount of heat loss due to conduction inside the chamber, evaluating heat loss primarily due to conduction. It was assumed that in the Cerakwool-filled case, only conduction was present as the heat transfer mechanism, and this value was used as the baseline for conduction heat loss in the other experimental cases. The vacuum condition of 0.07 bar was adopted for the vacuum case, as used in NuScale's VOYGR. In this scenario, heat loss was assumed to occur only due to conduction and radiative heat transfer.

In terms of methodology, gas was first injected at room temperature, and to minimize the influence of air, the gas injection and vacuum pump evacuation were repeated three times. Then, power was supplied to the heater using a DC power supply. The experiment was considered to be in a steady state when the calculated surface temperature of the conductor remained within ±0.2°C for 15 minutes, and the temperature of all

components stayed within 0.05°C. The experiment was then concluded.

Direct measurement with thermocouples posed difficulties due to attachment issues when measuring the surface temperature of the heater conductor. Therefore, the heat transfer rate was calculated using temperature measurements in the radial direction, and the surface temperature of the heater conductor was back-calculated using this heat transfer rate.

The test matrix and the equations used are summarized in the table below.

Table I: Test matrix

Heater Surface Temperature	~ 320 °C
Ambient Temperature	20 °C
Initial Pressure	0.07 bar (Cerakwool, Vacuum)
	1.00 bar (Nitrogen, Argon)
Gap condition	Cerakwool
	Vacuum
	Nitrogen
	Argon

Table II: Used formula

Temperature profile in cylindrical coordinates (Radial direction)
$T(r) = \frac{T_i - T_o}{\ln\left(\frac{r_i}{r_o}\right)} \ln\left(\frac{r}{r_o}\right) + T_o$
Heat transfer rate in cylindrical coordinates (Radial direction)
$q_r = -\frac{2\pi L \int_{T_i}^{T_o} k(T)dT}{\ln\left(\frac{r_o}{r_i}\right)}$
Radiative heat transfer rate in cylindrical enclosure
$q_{1-2,rad} = \frac{\sigma(T_1^4 - T_2^4)}{\frac{1}{A_1\varepsilon_1} + \frac{1-\varepsilon_2}{A_2\varepsilon_2}}$

3. Result

This section presents the experimental and analysis results for each gap-filling case. The power applied through the DC power supply in each case is shown in the following table.

Table III: Power applied via DC supply for each case

	Voltage (V)	Current (A)	Power (W)
Cerakwool	35.5	3.41	121.055
Vacuum	60.4	5.82	351.528
Nitrogen	76.2	7.32	557.784
Argon	71.9	6.89	495.391

3.1 Cerakwool case

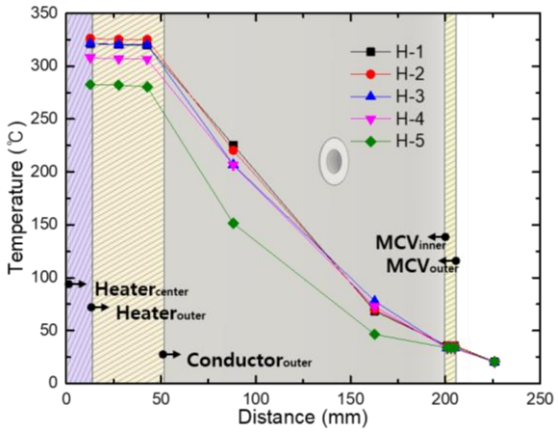

Fig. 4. Temperature distribution of the Cerakwool gap condition based on distance from the center and height (H-1: Top of chamber, H-5: Bottom of chamber)

Fig. 4 shows the temperature distribution by distance for the Cerakwool case. Due to the lower power input, the temperature gradient at the heater conductor and the chamber wall was smaller than in other cases. The heat from each component is calculated using the temperature measurement data, as shown in the following table.

Table IV: Calculated heat from each component (Cerakwool)

Heater Conductor (Radial direction)	Heat loss to the ambient		
	MCV	Flange	Total
100.988 W	94.974 W	25.924 W	120.898 W

When calculating the heat balance, it was found that approximately 83% of the heat applied through the DC power supply was conducted radially through the heater conductor, suggesting that some heat was lost axially. Additionally, based on the measured temperatures, the calculated heat loss to the ambient environment was slightly less than the heat supplied by the DC power. This discrepancy is likely due to thermocouple measurement errors and the bulk calculation of each component rather than dividing them into more precise sections.

Furthermore, as shown in Fig. 4, despite filling the gap with Cerakwool insulation, a temperature gradient was observed between the heater conductor and the chamber wall. By using the thermal conductivity of Cerakwool, the conductive heat transfer through the Cerakwool was calculated to be 43.484 W. Therefore, the heat transfer through conduction to the MCV in all cases was assumed to be 51.49 W, which is the difference between the total conduction heat transfer

(94.974 W) and the heat transferred through Cerakwool (43.484 W).

Using this information, the heat loss to the MCV due to the heat transfer mechanisms in the Cerakwool case is calculated as shown in the table below.

Table V: Heat loss to the outside air from the MCV due to different heat transfer mechanisms (Cerakwool)

Conduction	Convection	Radiation	Total
94.974W	-	-	94.974W

3.2 Vacuum case

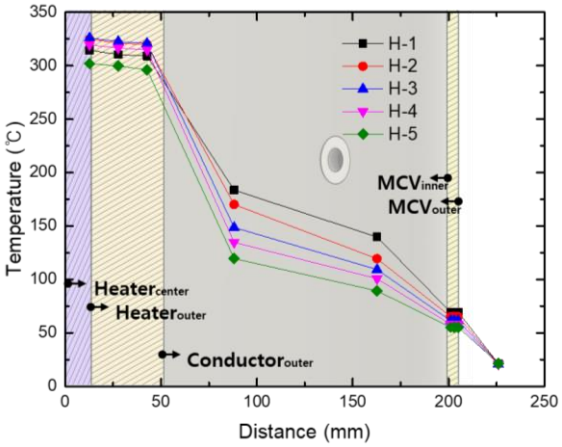

Fig. 5. Temperature distribution of the Vacuum gap condition based on distance from the center and height
(H-1: Top of chamber, H-5: Bottom of chamber)

Fig. 5 shows the temperature distribution by distance for the Vacuum case. Due to the vacuum's insulating effect, higher temperatures were observed around the heater conductor compared to gas-filled conditions. However, because natural convection effects are minimal in the vacuum, lower temperatures were measured in the gap closer to the chamber wall compared to gas-filled conditions. The heat from each component is calculated using the temperature measurement data, as shown in the following table.

Table VI: Calculated heat from each component (Vacuum)

Heater conductor (Radial direction)	Heat loss to the ambient		
	MCV	Flange	Total
340.920 W	287.288 W	57.744 W	345.024 W

In this experiment, the emissivity of each component was not measured. As mentioned earlier, it was assumed that there was no heat loss through convective heat transfer for the vacuum case. Based on the experimental results from the vacuum case, the emissivity of the heater conductor and the chamber wall were back-calculated and assumed. Specifically, it was assumed that radiative heat loss amounted to 235.798 W, the total heat through the MCV (287.288 W) minus the heat conducted (51.49 W). Consequently, in all cases, the emissivity of 0.2 for the heater conductor and 0.59 for the chamber wall were assumed and used for the radiative heat transfer calculations.

Using this information, the heat loss to the MCV due to the heat transfer mechanisms in the Vacuum case is calculated as shown in the table below.

Table VII: Heat loss to the outside air from the MCV due to different heat transfer mechanisms (Vacuum)

Conduction	Convection	Radiation	Total
51.49W	-	235.638W	287.128W

3.3 Nitrogen case

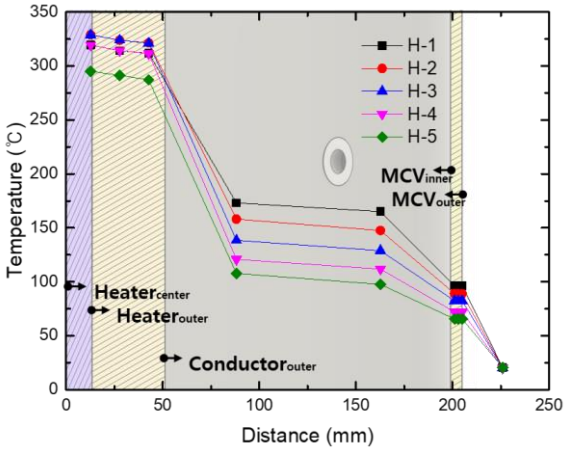

Fig. 6. Temperature distribution of the Nitrogen gap condition based on distance from the center and height
(H-1: Top of chamber, H-5: Bottom of chamber)

Fig. 6 shows the temperature distribution by distance for the nitrogen case. In the nitrogen case and the subsequent argon gas-filled condition, it was observed that the temperature gradient near the heater conductor and the gap close to the chamber wall was not significantly different due to natural convection within the chamber. However, the higher thermal conductivity of nitrogen led to more significant heat loss from the heater conductor to the gap compared to other cases. The heat from each component is calculated using the temperature measurement data, as shown in the following table.

Table VIII: Calculated heat from each component (Nitrogen)

Heater conductor (Radial direction)	Heat loss to the ambient		
	MCV	Flange	Total
508.827W	384.513W	129.897W	514.41W

Using this information, the heat loss to the MCV due to the heat transfer mechanisms in the Vacuum case is calculated as shown in the table below.

Table IX: Heat loss to the outside air from the MCV due to different heat transfer mechanisms (Nitrogen)

Conduction	Convection	Radiation	Total
51.49W	111.794W	220.804W	384.088W

3.4 Argon case

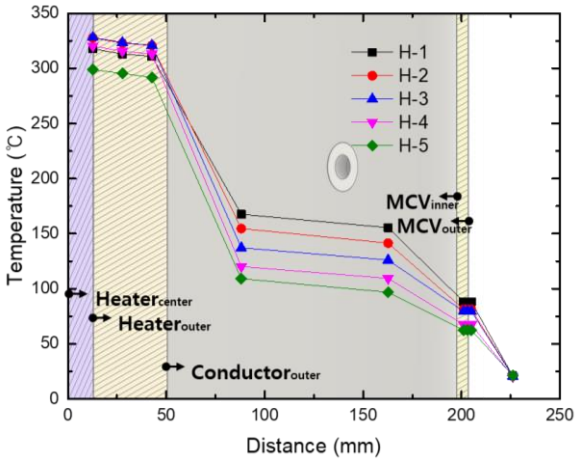

Fig. 7. Temperature distribution of the Argon gap condition based on distance from the center and height
(H-1: Top of chamber, H-5: Bottom of chamber)

Fig. 7 shows the temperature distribution by distance for the argon case. The heat from each component is calculated using the temperature measurement data, as shown in the following table.

Table X: Calculated heat from each component (Argon)

Heater conductor (Radial direction)	Heat loss to the ambient		
	MCV	Flange	Total
462.985W	372.045W	101.986W	474.026W

Using this information, the heat loss to the MCV due to the heat transfer mechanisms in the vacuum case is calculated as shown in the table below.

Table XI: Heat loss to the outside air from the MCV due to different heat transfer mechanisms (Argon)

Conduction	Convection	Radiation	Total
51.49W	95.343W	225.207W	372.04W

4. Discussion & Conclusion

4.1 Discussion

Comparing the heat applied via the DC power supply, the order of heat loss is as follows: Cerakwool < Vacuum < Argon < Nitrogen. Since the heater conductor temperature was fixed in this study, the Cerakwool case exhibits the lowest heat loss due to insulation and conduction alone. In the vacuum case, heat loss occurs through conduction and radiation with minimal convective heat transfer, resulting in relatively lower power usage compared to the scenario with a gas-filled gap at atmospheric pressure.

In gas-filled conditions, such as with nitrogen and argon, heat loss occurs due to conduction, convection, and radiation, leading to higher power consumption compared to Cerakwool and vacuum cases. Among these, nitrogen shows higher power consumption than argon due to its higher thermal conductivity, resulting in more significant heat loss near the heater conductor.

Heat loss at the upper and lower flanges is higher in gas-filled conditions than in the vacuum and Cerakwool cases. This is attributed to the relatively higher temperature gas moving to the upper flange due to internal natural convection.

4.2 Conclusion

This study conducted experiments to evaluate heat loss mechanisms to the external environment during normal reactor operation based on different gap conditions in SMR design. According to previous literature, radiative heat transfer was identified as the dominant heat loss mechanism for the RPV under steady-state conditions. Consequently, the experimental setup and temperature settings were designed considering the view factor at the pressurizer height of the reactor model.

The experimental results confirmed that the heat loss followed the nitrogen, argon, vacuum, and Cerakwool order from highest to lowest. It was also found that, except for the Cerakwool case, which assumed only conductive heat loss, radiative heat transfer was the dominant mechanism in all cases (ranging from a minimum of 57% to a maximum of 81%).

Overall, this study provides insights into the heat transfer mechanisms to the exterior of the RPV during normal operation in SMRs with MCV design, considering different gap conditions.

5. Acknowledgement

This study was sponsored by the Korea Hydro & Nuclear Power Co.'s affiliated Central Research Institute (KHNP-CRI). Additionally, this work was supported by the Human Resources Development of the Korea Institute of Energy Technology Evaluation and Planning (KETEP) grant funded by the Korea government Ministry of Knowledge Economy (RS-2024-00439210).

REFERENCES

[1] M.D. Carelli et al., "Economic features of integral, modular, small-to-medium size reactors," Progress in Nuclear Energy, 52 (4), pp. 403-414 (2010).
[2] D.T. Ingresoll et al., "NuScale small modular reactor for Co-generation of electricty and water," Desalination, 340, pp. 84-93 (2014).
[3] Reyes Jr, José N. "NuScale plant safety in response to extreme events." Nuclear Technology 178.2 (2012): 153-163
[4] Energy, GE Hitachi Nuclear. "BWRX-300 General Description." (2023)
[5] ARC CLEAN TECHONOLOGY
[6] Kumar, G. Vijaya, et al. "Implementation of a CFD model for wall condensation in the presence of non-condensable gas mixtures." Applied Thermal Engineering 187 (2021): 116546.
[7] Du, Wang-Fang, et al. "Numerical simulation and parameter sensitivity analysis of coupled heat transfer by PCCS containment wall." Applied Thermal Engineering 113 (2017): 867-877.
[8] Lee, Geon Hyeong, et al. "Analysis of heat-loss mechanisms with various gases associated with the surface emissivity of a metal containment vessel in a water-cooled small modular reactor." Nuclear Engineering and Technology (2024).